47th AIAA Aerospace Sciences Meeting Including The New Horizons Forum and Aerospace Exposition
5 - 8 January 2009, Orlando, Florida

AIAA 2009-1513

Perturbation Energy Production in Pipe Flow over a Range of Reynolds Numbers using Resolvent Analysis

A. S. Sharma,* B. J. McKeon†

The response of pipe flow to physically realistic, temporally and spatially continuous (periodic) forcing is investigated by decomposing the resolvent into orthogonal forcing and response pairs ranked according to their contribution to the resolvent 2-norm. Modelling the non-linear terms normally neglected by linearisation as unstructured forcing permits qualitative extrapolation of the resolvent norm results beyond infinitesimally small perturbations to the turbulent case. The concepts arising have a close relationship to input-output transfer function analysis methods known in the control systems literature. The body forcings that yield highest disturbance energy gain are identified and ranked by the decomposition and a worst-case bound put on the energy gain integrated across the pipe cross-section. Analysis of the spectral variation of the corresponding response modes reveals interesting comparisons with recent observations of the behavior of the streamwise velocity in high Reynolds number (turbulent) pipe flow, including the importance of very long scales of the order of ten pipe radii, in the extraction of turbulent energy from the mean flow by the action of turbulent shear stress against the velocity gradient.

I. Introduction

Predicting the structure of turbulent wall-bounded flows is a topic of intense fundamental and applied interest, yet, in general, understanding has advanced through experimental studies rather than theory due to the multi-scale nature of these flows. This is especially true at high Reynolds numbers, where for example recent work[1–4] has revealed the previously unexplained contribution of very large streamwise scales to the variance of the streamwise velocity and turbulent energy production via the shear stress, both of which increase with increasing Reynolds number.

A. Non-normality and algebraic disturbance growth

In this paper, we explore the insight into turbulent energy production offered by an analysis of the non-normal linear operator arising from linearization of the Navier-Stokes equations around the laminar velocity profile, an exact solution. We examine the variation of the resolvent norm, a measure of the algebraic growth of disturbances that is possible because of the non-normality, in wavenumber and temporal frequency space. It is proposed that the volume forcing implied by the resolvent norm analysis of the system linearised about the laminar velocity profile is supplied by the non-linearity 'feeding back' into the linearised equations. As a result, we expect regions in wavenumber and frequency space that have high resolvent norms to dominate the turbulent energy. This hypothesis provides a bridge from linear input-output analysis to experimental studies.

An operator A is non-normal if $AA^* \neq A^*A$ where A^* denotes the adjoint of A. Flows can yield highly non-normal operators when linearised about a steady flow solution with shearing. In the past fifteen years, significant progress has been made in understanding system non-normality as a mechanism for energy amplification in shear flows[5–7] leading to non-linear breakdown in both linearly stable and unstable flows.[8] It has been shown[9] that linear non-normality is required to sustain turbulence. Attempts have been made to use

*Departments of Electrical and Electronic Engineering, Aeronautics, Imperial College, London SW7 2AZ, United Kingdom
†Graduate Aeronautical Laboratories, California Institute of Technology

linear analysis to explain the dominant features of turbulent flow in terms of optimal transient modes[5,10] or stochastic forcing.[11,12] The present analysis is closer to a resolvent or system norm analysis.[13,14] A different approach by other authors[15–17] has developed exact solutions of the Navier-Stokes equations, giving rise to unstable coherent structures, as the foundations of transitional flow and/or near-wall turbulence.

If turbulence in pipe flows is to be a self-sustaining process, there must be a ready source of the turbulent energy to counter dissipation, which is provided by the interaction of low speed fluid with higher speed fluid. This process is captured by the linearised transport term in a linearisation around the laminar profile, the equivalent action of the Reynolds shear stress against the turbulent mean velocity profile. This term is entirely responsible for the non-normality of the linearised Navier-Stokes operator. As such, the energy amplification, like the dissipation, is a understandable as a linear process, and can be quantified by the non-normality of the linearised operator. In the sequel, this quantification is done via an analysis of the operator norms. As such we analyse this linear amplification process not as an initial value problem, but as a response to a body forcing provided by the discarded non-linear term. We do not seek here to model this forcing in detail, but satisfy ourselves merely by analysing the linear response to plausible components of that forcing that provide the greatest sustained energy production. It transpires that some modes have responses many orders of magnitude above the lower-responding modes. Given the complexity of turbulent flow, it seems reasonable to suppose that these modes will be excited and thus will be prominent in turbulent flow, allowing for an as yet undetermined limitation on the input forcing.

The forcing due to the perturbation equation non-linearity serves to transfer energy between wavenumbers but is not directly responsible for the energy gain (the non-normality). The non-normality comes from the non-linear term *linearised about the base flow*, reflecting the energy gain attainable from transport between areas of low steady flow velocity to those of high velocity. In this sense, saying that the energy gain available in shear flows is a linear or non-linear effect can be confusing. This simple point results in a difference of viewpoints about whether the non-normality is a linear versus non-linear effect that essentially can be considered nothing more that a semantic difference.

Though it is also an analysis of non-normality, the initial value problem examines the growth in time of a particular perturbation in the linearised equations. This approach assumes no continuous forcing from the non-linearity or external disturbance. Del Álamo & Jiménez[10] have shown that an initial value analysis based on linearization around the turbulent mean profile in channel flow indicates large energy amplification for solutions that resemble both the near-wall and large-scale structures observed in turbulent flows, and their respective scaling.

The current approach does not capture structural dynamics, but does give a qualitative representation of the scaling and distribution of energy production. Because the non-normality in the flow of interest is so pronounced, however, the two methods may often present similar modes, despite their differing interpretations.

Given the availability of both a highly accurate and accessible linear code[14] and experimental data,[2,18,19] Hagen-Poiseuille (pipe) flow is chosen to illustrate this analysis. For their resolvent analysis the authors of the code[14] claim the code is sufficiently accurate even up to $Re \sim 10^7$ given sufficient resolution. The current authors have found no evidence to dispute this despite extensive use of the code.

B. Equations for laminar flow in a pipe

A sketch of the coordinate system is given in Figure 1. The Reynolds number in the pipe with diameter $D = 2a$ is defined by

$$Re_l = \frac{\Pi a^3 \rho}{4\mu^2} \tag{1}$$

in order to maintain unit centerline velocity, where $-\Pi$ is the axial pressure gradient and $\nu = \mu/\rho$ is the kinematic viscosity. This expression is equivalent to the Reynolds number based on diameter and bulk velocity, *i.e.* , $Re = WD/\nu = Re_l$. In what follows, it will be assumed that at a given condition constant mass-flux is maintained in the pipe, independent of the laminar or turbulent state of the flow, such that Re can be used to reference a particular flow condition.

II. Methodology

A. Linearisation around the laminar velocity profile

We begin the mathematical treatment by considering perturbations $v(x,t)$ with x a point in the pipe interior Ω and time t, to a steady solution to Navier-Stokes equations $V(x,t)$ subject to no-slip boundary conditions. All variables are non-dimensionalised with respect to the centerline velocity, W, and the pipe radius.

The perturbation equations, with an externally applied forcing r that may be from acoustic forcing, wall roughness, etc., can be written as[20]

$$\dot{v}(x,t) = \mathcal{L}v(x,t) + \xi(x,t) + r(x,t) \tag{2}$$

$$\xi(x,t) = -v(x,t) \cdot \bigtriangledown v(x,t) \tag{3}$$

where the pressure variable and divergence equation have been eliminated by projection of the velocity field onto a divergence-free manifold and the linear operator $\mathcal{L}$ is given by

$$\begin{pmatrix} \frac{1}{R}(D^2 + \frac{1}{r}D - n^2r^{-2} - k^2 - r^{-2}) - ik\bar{W} & -2inr^{-2} & 0 \\ 2inr^{-2} & \frac{1}{R}(D^2 + \frac{1}{r}D - n^2r^{-2} - k^2 - r^{-2}) - ik\bar{W} & 0 \\ -D\bar{W} & 0 & \frac{1}{R}(D^2 + \frac{1}{r}D - n^2r^{-2} - k^2) - ik\bar{W} \end{pmatrix} \tag{4}$$

with the components of $v(x,t)$ being radial, azimuthal and axial velocities respectively. Note that Equation 2 is linear in v. Non-linear effects are introduced through the action of ξ. We lump together ξ with the external forcing r as $f = r + \xi$.

B. Spectral representation and resolvent

We analyze the amplification of traveling wave solutions. By Fourier transformation of Equation 2 in both the streamwise and azimuthal directions and Laplace transformation in time, the velocity can be written as a combination of orthogonal modes. The azimuthal constraints of the pipe mean that only integer azimuthal wavenumber n must be considered, while we expect that downstream traveling disturbances experience much larger amplification than upstream ones[21] such that we consider streamwise wavenumber k and frequency ω of opposite sign (but drop the negative sign in what follows).

$$v(x,t) = \frac{1}{2\pi i}\sum_n \int_{-i\infty}^{i\infty}\int_{-\infty}^{\infty} \hat{v}(k,n,s)e^{ikx+in\theta+st}\mathrm{d}k\mathrm{d}s. \tag{5}$$

Where relevant, the norm used is the usual perturbation energy ($\mathcal{L}_2(\Omega)$) norm.

The linearisation and spectral representation allows

$$\hat{v}(k,n,s) = (sI - \mathcal{L})^{-1}\hat{f}(k,n,s) \tag{6}$$

where the operator of interest $(sI-\mathcal{L})^{-1}$ is called the resolvent. The $\hat{\cdot}$ notation will be dropped in the sequel.

Note that reversal of sign of k has the same effect on the resolvent as the reversal of sign of ω, namely a reflection of the eigenvalues of $\mathcal{L}$ on the real axis.

C. Choice of profile for linearisation

When performing linear stability analysis by perturbation, the linearisation must occur around a solution to the equations that is steady (*i.e.* has zero time derivative or, if an approximation about differing timescales of the profile and the dynamics is to be made, almost zero).[22] This fixed point may or may not turn out to be stable to infinitesimally small perturbations. A harmonic forcing analysis requires similar considerations to linear stability arguments, so it is important that the flow is linearised around a steady solution to the full equations. A laminar profile, even if unstable, satisfies this requirement. However a mean turbulent profile does not, because were it ever instantaneously realised it would not be close to a steady solution.

Since the turbulent mean profile is not a steady solution to the Navier-Stokes equations, it is likely that any behaviour of a perturbation around that profile will be swamped by the dynamics of the profile itself (note however the success of, e.g. del Álamo & Jiménez[10] in predicting turbulent structure in channel flow using temporal stability analysis of the turbulent mean profile). Indeed we expect the dominant modes of the laminar profile to pick out the response to some posited unstructured forcing, which in a qualitative sense should generate the features dominant in the turbulent flow. Consequently, for our analysis of energy production we choose to linearise about the laminar profile. The results will differ between choice of profiles to the extent that the coupling between the radial and axial velocities, specifically the term $-DU$ in (4), changes. In any case, in both profiles the shearing leading to production occurs predominantly close to the wall, where the velocity gradient is largest.

The concept of Navier-Stokes as linear equations with non-linear 'feedback' has been raised in a control theory context[20] where passivity arguments were used for stability and control arguments. The emphasis here differs and is more toward the receptivity of the flow, defined as the the magnitude of response to forcing. In this view, the linear system receives some small forcing, resulting in an energetic velocity field. This flow field provides new forcing via the non-linearity, some of which the flow may be particularly receptive to, completing the cycle. In concept, it is similar to the 'mother-daughter' scenario of Boberg and Brosa,[23] where a linear but non-normal process allows small disturbances to feed more energetic disturbances that can dissipate the gained energy. Non-linear effects then transfer some of this energy to the smaller initial disturbances.

The understandings differ to the extent that the 'mother-daughter' scenario considers the evolution of structural perturbations, and naturally leads to the transient growth problem of Butler and Farrell[5] and others, whereas the presented viewpoint considers the gain response to harmonic forcing, naturally leading to a linear input-output analysis without a natural timescale.

D. Pseudospectra and the Schmidt decomposition of the resolvent

We seek a decomposition of the resolvent at a particular wavenumber pair and frequency which ranks the response to forcing in some sense. Considering just harmonic forcing restricts us to positive real frequency, $s = i\omega,\ \omega \in \mathbb{R}^+$. We take the Schmidt decomposition (called the singular value decomposition in the discrete case) of the resolvent

$$(i\omega I - \mathcal{L})^{-1} = \sum_{j=1}^{\infty} \psi_j(k,n,y,\omega)\sigma_j(k,n,\omega)\phi_j^*(k,n,y,\omega) \tag{7}$$

with an orthogonality condition

$$\int_y \phi_l(k,n,y,\omega)\phi_m(k,n,y,\omega)\mathrm{d}y = \delta_{lm} \tag{8}$$

$$\int_y \psi_l(k,n,y,\omega)\psi_m(k,n,y,\omega)\mathrm{d}y = \delta_{lm} \tag{9}$$

$$\sigma_l \geq \sigma_{l+1} \geq 0. \tag{10}$$

The ϕ_j and ψ_j form the right and left Schmidt bases for the forcing and velocity fields. The real σ_j are the singular values. This decomposition exists if there are no eigenvalues of $\mathcal{L}$ with zero real part and is unique up to a pre-multiplying complex factor on both bases of magnitude unity, corresponding to a spatial phase shift of both forcing and response, and up to the ordering of the σ_j's.[24]

This basis pair can then be used to decompose arbitrary forcing and the resulting velocity at a particular Fourier component

$$f(k,y,n,\omega) = \sum_{l=1}^{\infty} \phi_l(k,n,y,\omega)a_l(k,n,\omega) \tag{11}$$

$$v(k,n,y,\omega) = \sum_{l=1}^{\infty} \sigma_l(k,n,\omega)\psi_l(k,n,y,\omega)a_l(k,n,\omega). \tag{12}$$

The energy of the same Fourier component of the resulting disturbance velocity is

$$E(k,n,\omega) = \int_y v^*(k,n,y,\omega)v(k,n,y,\omega)\mathrm{d}y = \sum_{l=1}^{\infty} \sigma_l^2(k,n,\omega)a_l^2(k,n,\omega) \tag{13}$$

Clearly the forcing shape that gives the largest energy at a particular frequency and wavenumber is given by $a_{l\neq 1} = 0$. This approach permits the investigation of the dependence of maximum energy amplification on the form of the forcing in the wavenumber and frequency domain. Singular values for a given wavenumber pair and frequency correspond to full volume, three component forcing and response modes ranked by the receptivity of the linearized Navier-Stokes, which necessarily enforces zero (temporal) phase-shift between input and output. There is no requirement on the radial spatial phase, that is, the velocity response has the same k and n but not necessarily the same y distribution.

By Parseval's theorem, the energy integrated over frequency and wavenumber is equal to that integrated over time and the spatial domain (the spectral and physical spaces are isomorphic). As such, the 2-norm of the resolvent is the leading singular value, σ_1. This means that the normalised harmonic forcing that gives the largest disturbance energy in the $\mathcal{L}_2(\Omega \times [0,\infty))$ sense is $f = \phi_1$, with a 'gain' of σ_1. The next largest is $f = \phi_2$ and so on, at a particular wavenumber pair and frequency. The corresponding flow response modes are given by the related $v = \psi_1^*, \psi_2^*$, etc. For σ_j near zero, the modes are not easily computed because they are effectively degenerate. However for large σ_j the mode shapes are extremely robust to numerical error, as would be expected if these mode shapes are to be dominant under experimental conditions. We justify the use of this particular norm with the fact that the non-linear forcing is conservative in the perturbation energy.[20]

These concepts may be best understood in the context of the pseudospectra analysis of Trefethen[25] to show what we call the particular forcing and response receptivity modes, associated with large non-modal responses of a non-normal system. In this sense, this decomposition analyses the receptivity of the flow to forcing. In another sense, this decomposition examines the mode shapes associated with perturbations to the $\mathcal{L}$ operator (another pseudospectrum interpretation). Note that in the special case of a normal operator $\mathcal{L}$, the eigenvectors of the resolvent are coincident with the Schmidt bases found earlier.

The ϵ-pseudospectrum of $\mathcal{L}$, Λ_ϵ can be defined as

$$\Lambda_\epsilon(\mathcal{L}) = \left\{\lambda \in \mathbb{C} : (\lambda I - \mathcal{L})^{-1} \geq \epsilon^{-1}\right\}.$$

The pseudospectra are therefore the level curves of the resolvent. The spectrum of $\mathcal{L}$ is then the subset of the field of complex numbers where the resolvent is unbounded. This is shown graphically in the left pane of Figure 2. The pseudospectrum level curves are significant because they can be interpreted as bounds on the complex plane within which the spectrum of the perturbed operator lies. Where the pseudospectrum intrudes significantly on the right-half plane, significant perturbation growth with a nominally stable operator can result.[14] The resolvent norm, found as σ_1 in Equation 7, is equal to ϵ^{-1} at a particular point in the complex plane (*i.e.* the 'height' of a contour plot of the pseudospectrum).

By the maximum modulus principle, the maximum norm of the resolvent taken over the right half of the complex plane of a stable operator must lie on the boundary between the left and right half planes (the imaginary axis). Consequently we examine the value of the resolvent along the imaginary or $i\omega$ axis ($\mathrm{Re}(s) = 0$), corresponding to harmonic forcing. This is graphically interpreted as taking a slice of a pseudospectrum contour plot along the imaginary axis, as shown in Figure 2 for $k = n = 1$.

The resolvent also relates to the linear initial value problem. It is a consequence of the Hille-Yosida theorem[26] that the resolvent obeys

$$\|(\lambda I - \mathcal{L})^{-1}\|_2 \leq \frac{M}{p - w}$$

where p is the real part of λ, and M and w are real numbers and

$$\|e^{\mathcal{L}t}\|_2 = Me^{wt}.$$

M characterises the transient behaviour, and w the asymptotic response. It is an important open problem in control theory how to analytically determine M for a given w.[27]

E. Numerical procedure and resolution issues

Comparing the spectra for $Re = 10000$, $k = 0.5$, $n = 1$, for two different resolutions (Figures 3–4), we see that for $N = 63$ the spectrum is well resolved in the area shown and for $N = 20$ it is not. However the part of the spectrum nearly impinging on the imaginary axis of the complex s-plane remains reasonably well resolved even at this very low resolution. The third case (Figure 5) shows that for a more challenging $Re = 10^6$, with $k = 1,\ n = 1$, at $N = 300$ numerical problems dominate the spectrum. Consequently the resolvent norm evaluated over the imaginary axis $s = i\omega$ is reasonably accurate without necessarily requiring the full resolution of every eigenvalue. The main concern is numerical stability rather than under-resolution, where calculating the resolvent norm is the goal. In any case, one can never resolve the whole spectrum, since there are an infinitude of eigenvalues.

The magnitude and distribution with $i\omega$ of the resolvent appears to be relatively insensitive to under-resolution of the eigenvalue spectrum. While there is some variation at low values of σ (high and low ω), there is little effect on the location of the peak σ or the value of the broad plateau of high resolvent lying in the region $0.15 < i\omega < 0.95$. However increasing resolution beyond that permitted by the numerical accuracy leads to changes in the location and magnitude of peak values of the resolvent.

The effect of resolution on response/forcing mode shapes is less obvious than for the amplification. When the system is under-resolved, this is observed in the smoothness of the low velocity contours in the forcing mode and the spatial phase difference between forcing and response modes (and between components, with implications for shear stress), but with little effect on the mode shapes. Similar effects are observed for $\omega \neq 0$.

At each point in (Re, k, n, ω) space, a straightforward search procedure was performed to determine a resolution at which the calculation for the resolvent norm has converged. The point of convergence varies over the whole (Re, k, n, ω) space. Investigation shows that there is a plateau of convergence, before which the system is not well resolved and beyond which numerical instability problems begin to dominate, caused by the very non-normality we are trying to measure. For parameter values resulting in a less non-normal system these problems are less severe and convergence comes more cheaply. Examination of the mode plots at resolutions before, on and after the plateau confirm this view.

F. Classification of disturbances

Given some (unknown) forcing model for the real flow, as yet undetermined but perhaps derived from the known non-linearity, we anticipate that many forcing modes will be present in a real flow. The modes associated with high σ_i will be selected by the flow, as characterised by the resolvent (which is a *linear* process in turbulence) with some limitations based on the physical range of scales that are observed in experiments. The forcing due to the perturbation equation non-linearity (ξ) serves to transfer energy between wavenumbers but is not directly responsible for the energy gain (the non-normality). Recall that the non-normality and therefore the energy amplification, comes from the full non-linear term linearised about the base flow.

The longest energy-containing wavelengths that have been observed in turbulent pipe flow have been of order $kR \sim 10^{-2}$ in the streamwise direction, with a noticeable peak occurring for $kR \sim 10^{-1}$.[2] In this reference is determined from a spectral decomposition of temporal experimental data, using the local mean velocity as the convective velocity. This is equivalent to assuming a constant, linear dispersion relationship, often stated as Townsend's hypothesis of "frozen" turbulence in which the small scales are merely convected by the large scale velocity fluctuations. The validity of this hypothesis at the largest scales is not clear.

Therefore, in order to compare our results to experimental data, we classify modes by constant convective velocity, $U_c(y)$, where

$$U_c = \frac{\omega}{k}, \tag{14}$$

which is effectively a mapping from velocity to wall-normal position (which varies with Reynolds number and possibly also with scale k). Under this classification and assuming the validity of Taylor's hypothesis, the analysis determines the modes responsible for maximal energy gain at different wall-normal locations, while the observed energy at a given wall normal distance will be the integration of the most amplified mode shapes over all y. Note that a potential difficulty arises near the pipe centerline, since the laminar centerline velocity is maintained equal to one at all Reynolds numbers (*i.e.* the kinematic viscosity is used to change the

Reynolds number), while for turbulent flow under the constant-mass-flux assumption, the centerline velocity must drop as the Reynolds number increases.

We present our results in terms of contour maps of the value of $k\sigma_1^2$, *i.e.* , the maximum energy amplification corresponding to an input disturbance, *vs.* streamwise wavenumber and Reynolds number for given azimuthal wavenumbers and convective velocities. We will justify the former in the following treatment; the latter leads to the linear relationship between frequency and streamwise wavenumber. Note that in this premultiplied form, integration over k at a given n, Re, U_c corresponds to equal energy.

III. Results

A. Structure of the most amplified disturbances

1. *Amplification as $k \to 0$ and Re dependence*

Figures 6 and 7 show the forcing and response modes, respectively, for the streamwise constant $k = 0, n = 1$ case at $Re = 3.2 \times 10^4$, which is highly amplified ($\sigma_1 \approx 10^6$). Clearly this mode pair corresponds to a transfer and amplification of energy from the transverse velocity components to the axial velocity, in the form of streaks that span half the pipe area. It is well-known that the highest non-normal mode amplification occurs for streamwise constant modes and that this mechanism leads to cross-plane rolls and streamwise streaks. Similar phenomena have been observed in analyses using other norms in different flows[7, 12, 28] and it can be hypothesized that their existence is confirmed by the natural persistence of very long structures in observations – experimental and numerical – of, amongst other flows, turbulent pipe flow (see[1] and.[29]) Note, however, that the extent of these energetic structures observed from point measurements is closer to $10R$, although planar measurements have suggested a spanwise meandering of similar structures in boundary layer flow,[30] which could suggest longer base structures subject to deformation by turbulent fluctuations at other scales.

For all $U_c = \omega/k$ and all Re, we observe a region where $\sigma \sim Re^4$ for all sufficiently low k, *e.g.* Figures 8(a-f). In this regime, all disturbances for a given n and Re undergo the same amplification (that is, $\sigma(\omega, k, n, Re) = \sigma(n, Re)$). In the limit $k \to 0$, ω must also $\to 0$ to maintain a given phase speed, U_c and we approach the idealised case of streamwise constant disturbances. The region of constant amplification at low k rolls off at a wavenumber k_{RO} that varies with Reynolds numbers as Re^{-1} and n for all i investigated here.

There is no direct reason why we should expect the Re^3 dependence found by, e.g., Bamieh and Dahleh[12] for stochastically-forced channel flow. Jovanovic & Bamieh[13] use a stochastic forcing model because it is analytically tractable and also find an Re^3 dependence. Because we are dealing with an unstructured forcing model (the maximum or worst-case gain) the relevant operator norm is different and it is to be expected that the Re dependence is different. Also the present work uses a pipe geometry rather than the channel geometry of the other work.

2. *Variation of amplified modes with convective velocity*

For increasing convective velocity (loosely interpreted as distance from the wall), a second feature of the amplification curves becomes apparent. A point of inflection in the contours of constant amplification appears, following a wavenumber locus, k_{IN}, with an inverse dependence on the Reynolds number at a given height. For a given (n, Re) combination, this inflection first moves to lower wavenumber as the convection velocity (distance from the wall) is increased, until it is indistinguishable from the change in slope caused by the $k \to 0$ roll-off when $U \approx 0.50$. When the distance from the wall is further increased, the inflection weakens and moves towards higher wavenumbers. Examination of the forcing and response mode shapes in the wavenumber region associated with this inflection reveals that there is a transition in mode across the inflection. For $k < k_{IN}$, the mode shapes resemble the rolls and streaks observed for $k \to 0$ (Figure 7), becoming increasingly more localized in y when $k_{RO} < k < k_{IN}$ (Figure 9). In the region of $k = k_{IN}$ amplification is obtained by rotation of the forcing mode from the azimuthal component to a response in the axial velocity, while for $k > k_{IN}$, the forcing mode is increasingly dominated by the axial component for increasing k, leading to a response in all three velocity components.

We note that the maximum amplification indicated in Figures 8 across k is obtained when $U_c = 0.50$. Equating this convective velocity to the local laminar velocity suggests that this amplification occurs for $y/R \approx 0.3$, which is approximately the wall-normal location at which the turbulent and laminar velocities are equal for a range of Reynolds numbers for this constant mass-flux case.

We now perform a preliminary comparison of the most amplified modes to 'wall-' and 'center-' type modes. For the case $k = 1, n = 1$ at $Re = 10^5$ with $\omega = 0.02, 0.75, 0.9999$, give the mode shapes in Figures 10 to 12. The $\omega \sim 0$ case does indeed correspond to a near-wall mode, $\omega \sim 1$ is a center mode and $\omega = 0.75$ is somewhere in between, in support of Taylor's hypothesis for this condition. Note however that the amplification of the $\omega = 0.75$ case ($\sigma \sim 2000$) exceeds that of both the center mode ($\sigma \sim 500$) and the wall mode ($\sigma \sim 30$), despite the proximity of the eigenvalue corresponding to the center mode to the $i\omega$ axis. For example, Meseguer's values[14] for the rightmost eigenvalues for the wall and center modes at $Re = 10^5$ are given as, for the center mode, $\lambda_{RC} = -0.0072023080 + 0.9846498289i$ and for the wall mode $\lambda_{RW} = -0.0292364601 + 0.1372143077i$. However the resolvent norm indicates an approximately constantly high σ (at least in a logarithmic sense) between the ω values corresponding to the wall and center modes. This is at the heart of our study. It is not necessarily only the modes associated with eigenvalues closest to the axis that lead to the largest amplification.

The comparison of the resolvent norm with the normal spectrum deals to first order with the variation of amplification of a given wave number pair with varying wall-normal distance (through the relationship between ω, k and the convective velocity), while the surface plots shown here detail the relationship between convective velocity and peak amplification across k, hopefully of more relevance for extension to turbulent flow.

3. Effect of azimuthal wavenumber

The contours of constant σ_1 in the surface plots of figure 8 remain qualitatively the same shape for different values of n, with slightly differing contour values. The influence of the azimuthal wavenumber on the peak amplification is shown in Figure 13 for three different convective velocities at constant Reynolds number and streamwise wavenumber, $Re = 10^5$ and $k = 0.1$, which span the mode regimes described above for the values of U_c selected, and for four wavenumbers at constant $U_c = 0.19$ in figure 14. For constant U_c, the azimuthal wavenumber for maximum amplification clearly decreases with decreasing streamwise wavenumber. For constant k, n decreases with increasing convective velocity, with a clear maximum in the value of σ_1 for intermediate velocities.

B. Comparison with observed results

The analysis we present has shown the most geometrically-amplified disturbances to the laminar velocity profile, in an algebraic sense. Assuming that the change in the mean velocity profile correspond to a streamwise constant disturbance arising from the non-linearity, the question of the correspondence of the amplified modes to those observed in turbulent flow remains to be determined.

Without solving the full problem and knowing the wavenumber distribution of the non-linear forcing, *i.e.* the a_l's of equations (11) and (12), we must invoke physical considerations that act as a filter to reduce the response to the longest, non-physical wavelengths. As noted above, only finite length disturbances are observed in experimental studies of pipe flow where the test sections have been designed with consideration of the length required for the flow to be fully-developed, in the sense of vanishing streamwise gradient of the statistics. For example, measurements in the test section of the Princeton/ONR Superpipe[31] were all taken downstream of length $L \approx 164D$, corresponding to a wavelength $k_{long}R = 2\pi/328 \approx 2 \times 10^{-2}$, in good agreement with the lowest wavenumber at which there is non-negligible energy in the one-dimensional streamwise velocity spectrum at the higher Reynolds numbers.

The variation of peak amplification with azimuthal wavenumber and convective velocity for $k > k_{IN}$ agrees favorably with the variation of spanwise wavelength inferred from the study of Monty *et al*,[19] who plotted the variation of scale l_z with y/δ, where l_z is defined as the difference between the Δz values at which the correlation $R_{uu}(\Delta z) = 0.05$. Approximating the corresponding dominant spanwise wavelength, n, giving rise to this correlation, as $n \sim 3l_z$, we see that the correct increase with wall-normal distance is given in

Figure 13. That is, as the distance from the wall increases (and therefore so does the convective velocity,) the n for maximum amplification decreases, assuming a constant k. Disturbances for high k are localized in y.

That this analysis of the laminar profile does not yield a peak associated with the near-wall cycle (here and Reddy & Henningson for the channel) suggests either that the amplification of $k \to 0$ waves swamps the response corresponding to those structures in this analysis or that a different origin must be considered, with consideration of the change in the mean velocity profile. Another consequence of working with the laminar profile, is that a question arises as to how the mapping from convective velocity to wall-normal location changes because of the difference between the laminar and mean turbulent profiles.

IV. Conclusions

Analysis of the resolvent norm associated with the linearization about the laminar velocity profile in pipe flow leads to large-scale structures that have characteristics resembling those observed in experiments and simulations on turbulent pipe flow. We have modeled the non-linear terms as harmonic forcing of the linear operator. By comparison with the eigenvalue spectrum, we confirm that the most amplified mode shapes from the resolvent norm are not predictable from the proximity of the eigenvalues to the axis. However, for a fixed convective velocity, distinct changes in mode shape occur, ranging from modes that lead to streamwise streaks that span the pipe radius for $k \to 0$ to a localized response in all three components for large k. For $k \to 0$, Re^4 amplification is observed for this type of forcing.

The support of the UK EPSRC and an NSF-CAREER award No. 0747672 (Program Manager William W. Schultz) are gratefully acknowledged by A. Sharma and B. McKeon, respectively.

References

[1]Kim, J. and Lim, J., "A linear process in wall-bounded turbulent shear flows," *Phys. Fluids*, Vol. 12, No. 8, 1993, pp. 1885–1888.

[2]Morrison, J. F., Jiang, W., McKeon, B. J., and Smits, A. J., "Scaling of the streamwise velocity component in turbulent pipe flow," *J. Fluid Mech.*, Vol. 508, 2004, pp. 99–131.

[3]Hutchins, N. and Marusic, I., "Evidence of very long meandering features in the logarithmic region of turbulent boundary layers," *J. Fluid Mech.*, Vol. 579, 2007, pp. 1–28.

[4]Guala, M., Hommema, S. E., and Adrian, R. J., "Large-scale and very-large-scale motions in turbulent pipe flow," *J. Fluid Mech.*, Vol. 554, 2006, pp. 521–542.

[5]Butler, K. and Farrell, B., "Three-dimensional optimal perturbations in viscous shear flow," *Phys. Fluids*, Vol. 4, No. 8, 1992, pp. 1637–1650.

[6]Trefethen, L., Trefethen, A., Reddy, S., and Driscoll, T., "Hydrodynamic stability without eigenvalues," *Science*, Vol. 261, No. 5121, 1993.

[7]Farrell, B. and Ioannou, J., "Stochastic forcing of the linearized Navier-Stokes equations," *Phys. Fluids*, Vol. 5, No. 11, 1993, pp. 2600–2609.

[8]Jovanovic, M. R. and Bamieh, B., "Unstable modes versus non-normal modes in supercritical channel flows," *Proceedings of the 2004 American Control Conference*, Boston, MA, 2004.

[9]Henningson, D. and Reddy, S., "On the role of linear mechanisms in transition to turbulence," *Phys. Fluids*, Vol. 6, 1994, pp. 1396–1398.

[10]del Álamo, J. C. & Jiménez, J., "Linear energy amplification in turbulent channels," *J. Fluid Mech.*, Vol. 559, 2006, pp. 205–213.

[11]Farrell, B. F. and Ioannou, P. J., "Perturbation structure and spectra in turbulent channel flow," *Theor. Comput. Fluid Dynamics*, Vol. 11, 1998, pp. 237–250.

[12]Bamieh, B. and Dahleh, M., "Energy amplification in channel flows with stochastic excitation," *Phys. Fluids*, Vol. 13, No. 11, 2001, pp. 3258–3269.

[13]Jovanovic, M. R. and Bamieh, B., "Componentwise energy amplification in channel flows," *J. Fluid Mech.*, Vol. 534, 2005, pp. 145–183.

[14]Meseguer, A. and Trefethen, L. N., "Linearized pipe flow to Reynolds number 10^7," *J. Comp. Phys.*, Vol. 186, 2003, pp. 178–197.

[15]Waleffe, F., "On a self-sustaining process in shear flows," *Phys. Fluids*, Vol. 9, No. 4, 1997, pp. 883–900.

[16]Waleffe, F., "Exact coherent structures in channel flow," *J. Fluid Mech.*, Vol. 435, 2001, pp. 93–102.

[17]Waleffe, F., "Homotopy of Exact Coherent Structures in Plane Shear Flows," *Phys. Fluids*, Vol. 15, No. 6, June 2003.

[18]McKeon, B. J., Li, J., Jiang, W., Morrison, J. F., and Smits, A. J., "Further observations on the mean velocity distribution in fully developed pipe flow," *J. Fluid Mech.*, Vol. 501, 2004, pp. 135–147.

[19]Monty, J. P., Stewart, J. A., Williams, R. C., and Chong, M. S., "Large-scale features in turbulent pipe and channel flows," *J. Fluid Mech.*, Vol. 589, 2007, pp. 147–156.
[20]Sharma, A. S., McKeon, B. J., Morrison, J. F., and Limebeer, D. J. N., "Stabilising control laws for the incompressible Navier-Stokes equations using sector stability theory," *3rd AIAA Flow Control Conference*, June 2006.
[21]Morrison, W. R. B. and Kronauer, R. E., "Structural similarity for fully developed turbulence in smooth tubes," *J. Fluid Mech.*, Vol. 39, No. 1, 1969, pp. 117–141.
[22]Arrowsmith, D. K. and Place, C. M., "An Introduction to Dynamical Systems," 1990.
[23]Boberg, L. and Brosa, U., "Onset of Turbulence in a Pipe," *Zeitschrift fur Naturforschung*, Vol. 43a, 1988, pp. 697–726.
[24]Young, N., *An Introduction to Hilbert Space*, Cambridge University Press, Cambridge, UK, 1988.
[25]Trefethen, L. and Bau, D., *Numerical Linear Algebra*, Society for Industrial Mathematics, 1997.
[26]Curtain, R. F. and Zwart, H. J., *An Introduction to Infinite-Dimensional Linear Systems Theory*, Springer-Verlag, New York, 1995.
[27]Blondel, V. and Megretski, A., editors, *Unsolved Problems in Mathematical Systems and Control Theory*, Princeton University Press, 2004.
[28]Bobba, K., *Robust Flow Stability: Theory, Computations and Experiments in Near Wall Turbulence*, Ph.D. thesis, California Institute of Technology, 2004.
[29]Wu, X. and Moin, P., "A direct numerical simulation study on the mean velocity characteristics in pipe flow," *J. Fluid Mech.*, Vol. 608, 2008, pp. 81–112.
[30]Hutchins, N. and Marusic, I., "Large-scale influences in near-wall turbulence," *Phil. Trans. Royal Soc. A*, Vol. 365, 2007, pp. 647–664.
[31]Zagarola, M. V. and Smits, A. J., "Mean-flow scaling of turbulent pipe flow," *J. Fluid Mech.*, Vol. 373, 1998, pp. 33–79.

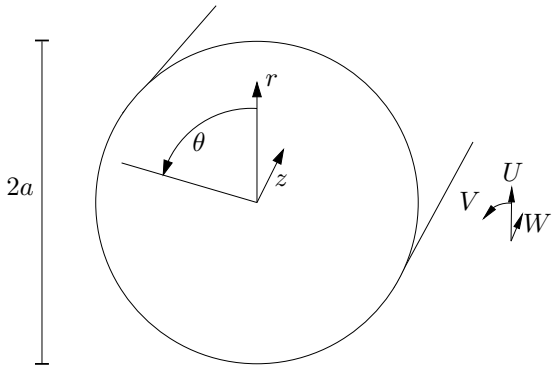

Figure 1. Schematic of pipe flow geometry.

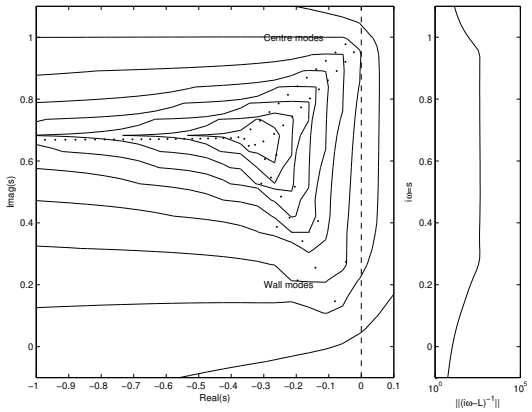

Figure 2. Spectrum, pseudospectrum and resolvent norm analysis for $k = 1$, $n = 1$, $Re = 10000$. Level curves at $(\lambda I - \mathcal{L})^{-1} = 10^1,\ 10^2,\ 10^3 \ldots$

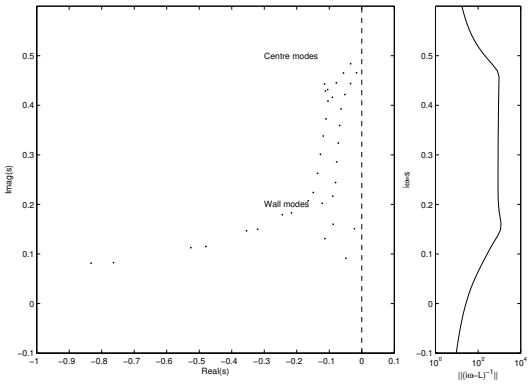

Figure 3. Under-resolved resolvent norm analysis for $Re = 10^4, k = 0.5, n = 1, N = 20$.

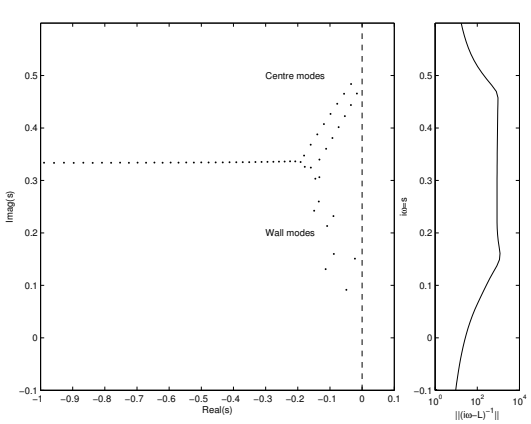

Figure 4. Well-resolved resolvent norm analysis for $Re = 10^4, k = 0.5, n = 1, N = 63$.

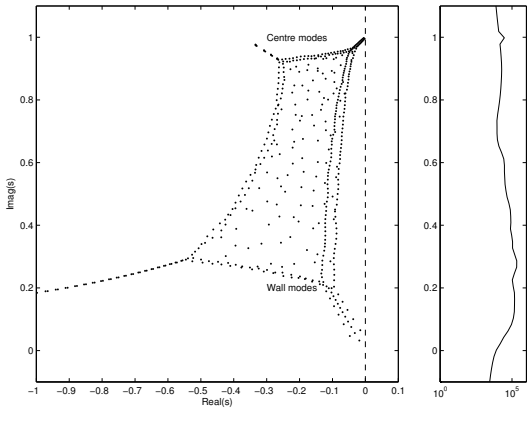

Figure 5. Poorly-resolved (due to numerical accuracy) resolvent norm analysis for $Re = 10^6, k = 1, n = 1, N = 300$.

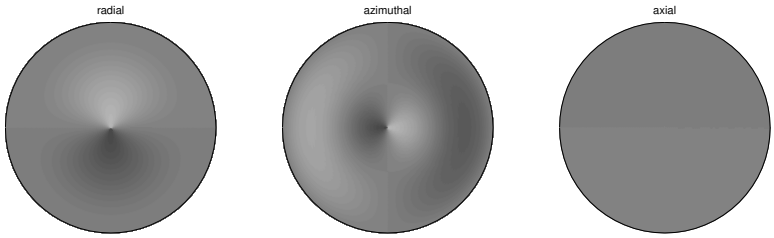

Figure 6. Forcing mode, ϕ_1, corresponding to $k = 0, n = 1, w = 0$ at $Re = 3.2 \times 10^4$.

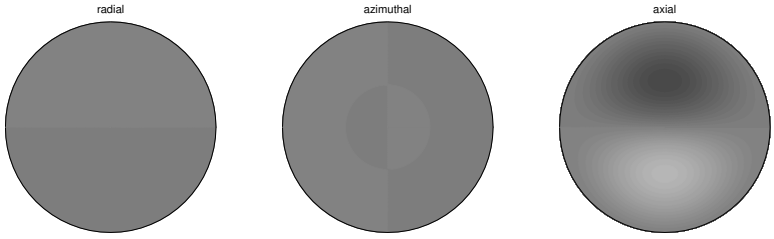

Figure 7. Response mode, ψ_1, corresponding to $k = 0, n = 1, w = 0$ at $Re = 3.2 \times 10^4$. $\sigma_1 \approx 10^6$.

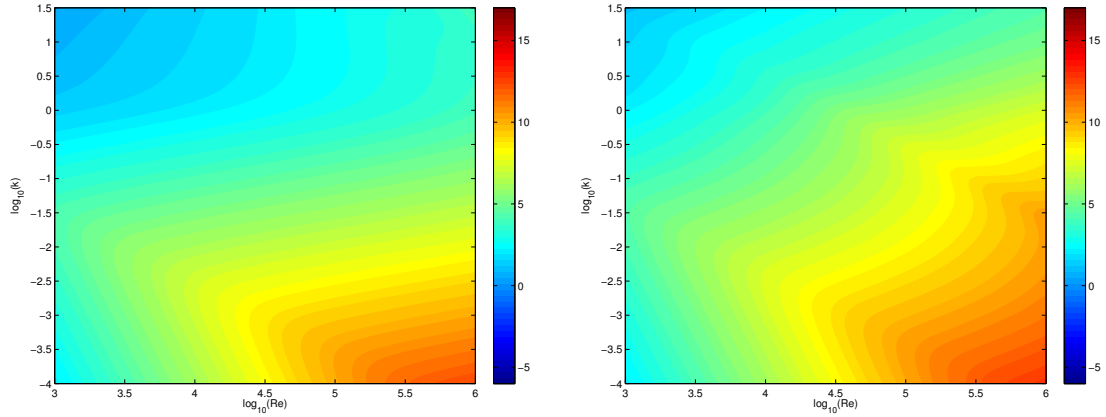

(a) $U = 0.02$ ($y_{laminar} = 0.01$).

(b) $U = 0.19$ ($y_{laminar} = 0.1$).

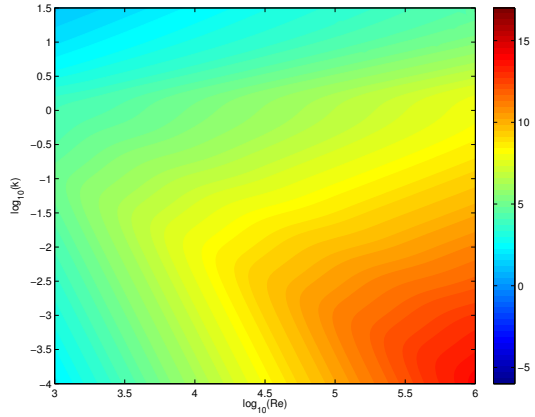

(c) $U = 0.51$ ($y_{laminar} = 0.3$).

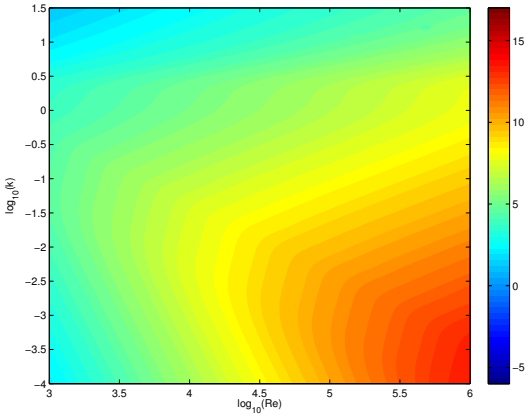

(d) $U = 0.75$ ($y_{laminar} = 0.5$).

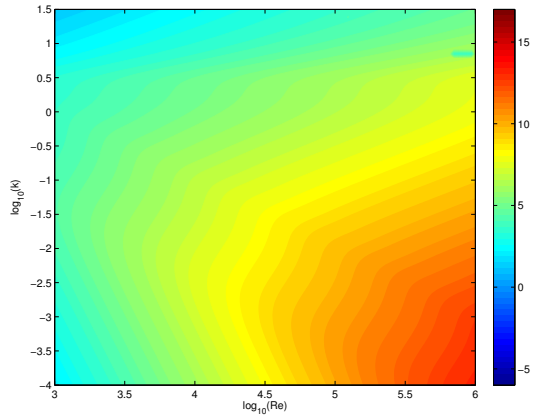

(e) $U = 0.84$ ($y_{laminar} = 0.6$).

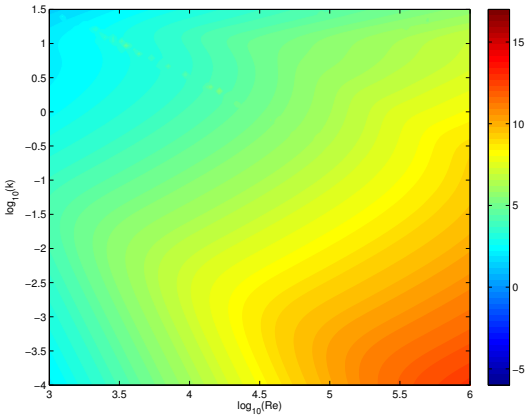

(f) $U = 0.99$ ($y_{laminar} = 0.9$).

Figure 8. Variation of $\log k\sigma_1^2$ with streamwise wavenumber k and Reynolds number for azimuthal wavenumber $n = 1$ and convective velocities $U = 0.02,\ 0.19,\ 0.51,\ 0.75,\ 0.84$ and 0.99, *i.e.* from close to the wall to close to the centerline in the laminar velocity profile.

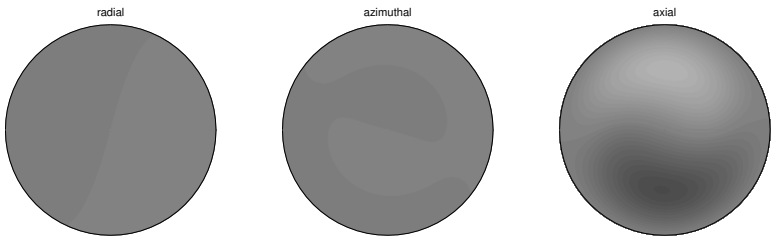

Figure 9. Response mode, ψ_1, corresponding to $k = 0.01, n = 1, \omega = 0$ at $Re = 10^4$.

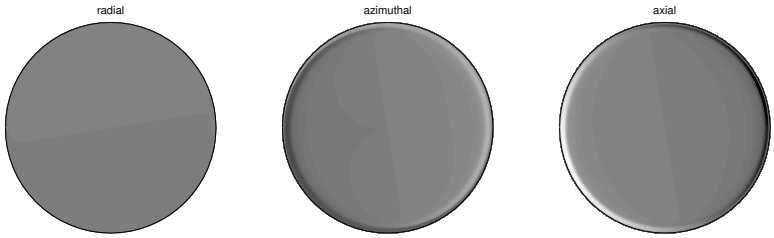

Figure 10. Response mode $1, k = 1, n = 1, \omega = 0.02, \sigma \sim 30, U_c = 0.02$. $Re_D = 10^5$.

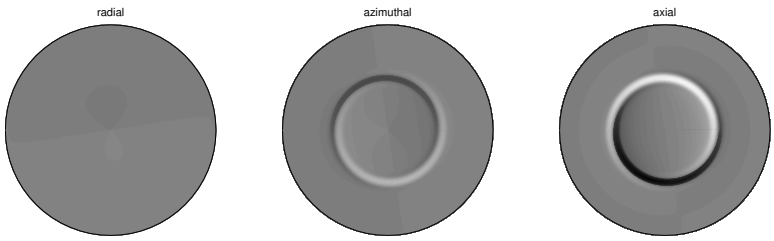

Figure 11. Response mode $1, k = 1, n = 1, \omega = 0.75, \sigma \sim 2000, U_c = 0.75$. $Re_D = 10^5$.

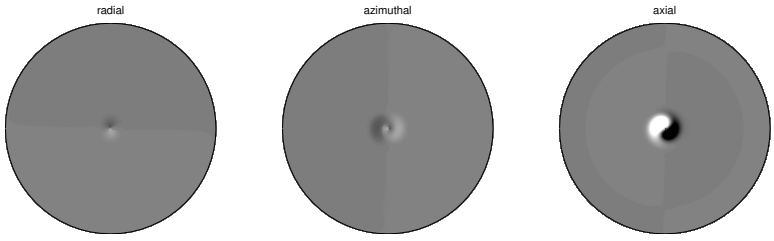

Figure 12. Response mode $1, k = 1, n = 1, \omega = 0.9999, \sigma \sim 500, U_c = 0.99$. $Re_D = 10^5$.

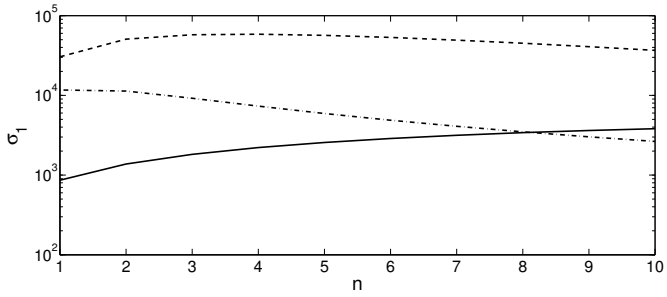

Figure 13. Effect of azimuthal wavenumber, n, on first singular value, σ_1, at $Re = 10^5$ and $k = 0.1$: $U_c = 0.01$ (solid), $U_c = 0.51$ (dashed) and $U_c = 0.99$ (dash-dotted).

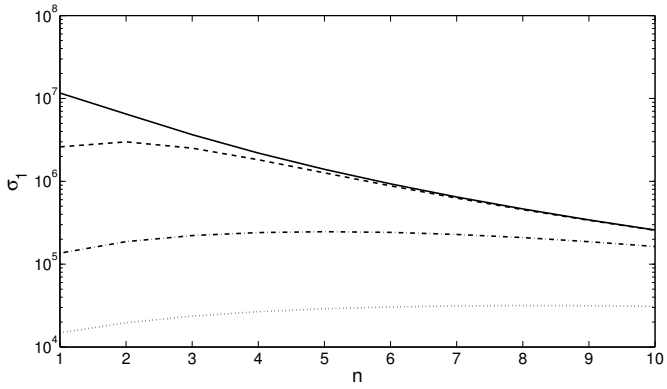

Figure 14. Effect of azimuthal wavenumber, n, on first singular value, σ_1, at $Re = 10^5$ and $U_c = 0.19$: $k = 10^{-4}$ (solid), $k = 10^{-3}$ (dashed), $k = 10^{-2}$ (dash-dotted) and $k = 10^{-1}$ (dotted), .